Model-based needle control in prostate percutaneous procedures

Arash Maghsoudi and Mehran Jahed

Proceedings of the Institution of Mechanical Engineers, Part H: Journal of Engineering in Medicine 2013 227: 58 originally published online 11 September 2012
DOI: 10.1177/0954411912458489

Original Article

Institution of MECHANICAL ENGINEERS
Journal of ENGINEERING IN MEDICINE

Proc IMechE Part H:
J Engineering in Medicine
227(1) 58–71

DOI: 10.1177/0954411912458489
pih.sagepub.com
SAGE

Model-based needle control in prostate percutaneous procedures

Arash Maghsoudi and Mehran Jahed

Abstract

In percutaneous applications, needle insertion into soft tissue is considered as a challenging procedure, and hence, it has been the subject of many recent studies. This study considers a model-based dynamics equation to evaluate the needle movement through prostate soft tissue. The proposed model estimates the applied force to the needle using the tissue deformation data and finite element model of the tissue. To address the role of mechanical properties of the soft tissue, an inverse dynamics control method based on sliding mode approach is used to demonstrate system performance in the presence of uncertainties. Furthermore, to deal with inaccurate estimation of mechanical parameters of the soft tissue, an adaptive controller is developed. Moreover, through a sensitivity analysis, it is shown that the uncertainty in the tissue mechanical parameters affects the system performance. Our results indicate that the adaptive controller approach performs slightly better than inverse dynamics method at the expense of fine-tuning the additional gain parameter.

Keywords

Needle insertion, tissue mechanical properties, inverse dynamics controller, adaptive controller

Date received: 29 December 2011; accepted: 3 July 2012

Introduction

Related works

In many modern medical procedures, needle insertion is an inevitable part of the diagnosis or the treatment protocols. In such procedures, a target deep inside the anisotropic, viscoelastic, inhomogeneous, and multilayered soft tissue must be reached via inserting needles. Procedures such as brachytherapy,[1] biopsy,[2] and neurosurgery[3] require accurate needle insertion techniques.

The effectiveness of the needle insertion is affected by a number of factors such as the flexibility of the needle that induces complex mechanical interactions and may result in considerable uncertainties. In addition, tissue deformation and rotation and consideration of the needle tip structure may contribute to further complexities.

Soft tissue modeling seems to be a crucial step in simulation studies of the needle insertion procedure. Finite element model (FEM) as a well-known solution to solid mechanics problems has been widely used for the simulation of the soft tissue behavior.[4,5] DiMaio and Salcudean[6] used a two-dimensional (2D), static and linear FEM model to represent a linearly elastic soft tissue. Alterovitz et al.[7] used a dynamic and linear FEM to model the soft tissue and thereby considered the mass of each element and velocity-dependent forces in the FEM formulation. Goksel et al.[8,9] used a three-dimensional (3D) FEM model of the prostate for the simulation of the prostate brachytherapy. Dehghan and Salcudean[10] simulated the prostate with a 3D FEM with the Neo-Hookean constitutive equation; however, this model was only used in simulation, while in experiments they utilized the linear FEM because of practical considerations of real-time implementation.

Many researchers have investigated the interaction force between the needle and tissue.[11–15] Simone and Okamura[12] devised an experimental setup to measure the forces involved during needle insertion in bovine liver and fitted a model to the measured data by dividing the interaction force into cutting forces, friction forces (using Karnopp stick–slip model[16]), and stiffness forces. DiMaio and Salcudean[17] estimated the force distribution along the needle using a homogeneous and

Robotics and Machine Vision Lab, School of Electrical Engineering, Sharif University of Technology, Tehran, Iran

Corresponding author:
Arash Maghsoudi, Robotics and Machine Vision Lab, School of Electrical Engineering, Sharif University of Technology, Tehran, 11365-11155, Iran.
Email: a_maghsoudi@ee.sharif.ir

Hookean 2D tissue phantom. By measuring the phantom deformation and using FEM model of the phantom, they calculated the force distribution and suggested two types of forces, namely, friction along the needle shaft and cutting force at the needle tip. They also reported that the shaft force depended on the needle velocity while the tip force was constant for different velocities. Crouch et al.[18] proposed a velocity-dependent force model for needle insertion based on the force measured while inserting needle into a tissue phantom at different velocities. Their model did not include the dependency of the forces of soft tissue mechanical properties. Dehghan et al.[19] used the ultrasonic tissue deformation data taken from a prostate phantom to find the distribution of the force along the needle shaft.

Due to the nonholonomic constrained movement of the needle into the tissue, many researchers have focused on the subject of "needle steering." DiMaio and Salcudean[20] introduced a Jacobian matrix to formulate the relationship between the needle tip and the needle base velocity. Alterovitz et al.[5,21] steered a bevel-tip needle inside a 2D tissue model under Markov uncertainty and optimized the insertion point of the needle using a search-based algorithm. They found the optimal depth by simulation of the needle at a given insertion height and chose the depth with minimum error. To find the optimal height they used a golden section search.[22] Alterovitz et al.[23] also found the optimal insertion point and angle for a flexible needle while avoiding the obstacles in the tissue. To solve the optimization problem, they used a penalty method in conjunction with gradient descent algorithm. Since their cost function was not directly differentiable, they used a perturbation method to find the approximation of the cost function differentiation. Webster et al.[24] formulated and experimentally validated a nonholonomic model governing the kinematics of a highly flexible bevel-tip needle. Park et al.[25] used the diffusion-based motion planning while considering the nonholonomic kinematics constraints for a highly flexible needle. Glozman and Shoham[26] used the inverse kinematics of a flexible needle inserted into a viscoelastic tissue model. They showed analytically that the trajectory of the needle base is not unique and that the optimization can be done by minimizing the lateral pressure of the needle body on the tissue. Dehghan and Salcudean[27] optimized the insertion point, angle, and depth in a 3D tissue model for multiple targets inside the tissue. Wood et al.[28] used the curvature of the flexible needle for kidney percutaneous medical interventions. To control the curvature of the flexible needle, they used the duty-cycled rotation of a bevel-tipped needle.

To highlight the role of the tissue mechanical properties in needle insertion procedures, some researchers performed a sensitivity analysis. DiMaio and Salcudean[20] examined the sensitivity of the needle tip positioning error to Young's modulus in their simulation studies. Alterovitz et al.[7] simulated the sensitivity analysis for Young's modulus in addition to other insertion parameters such as insertion point, velocity, and needle sharpness. They proposed that an increase in Young's modulus value decreases the error while changes in Poisson's ratio do not affect the error at all. To provide a more realistic model for prostate brachytherapy, Maghsoudi and Jahed[29] considered the anatomical constraint on the prostate tissue and applied the sensitivity analysis of the target-reaching error to tissue mechanical properties. Ophir et al.[30] used the ultrasonic elastography method to measure the soft tissue mechanical properties.

Problem realization and paper contribution

In this study, a control scheme for the needle insertion problem is proposed, which utilizes a tissue model to estimate the force applied to the needle. In the proposed approach, needle–tissue interaction forces are estimated by detecting the tissue deformation and evaluating the tissue model. In contrast to similar works,[19] this study does not reduce the force data by fitting a model to it; instead, it utilizes the model-based estimated force, distributed along the needle, as the force feedback in the control law and at the same time uses an adaptive controller to provide an update to the tissue mechanical properties in order to satisfy the control criteria. This article is organized as follows: section "Methods" provides a description of the methods used in this article including needle–tissue system, FEM-based force estimation, needle control formulation by inverse dynamics and adaptive controller, and simulation algorithm. Section "Results" presents the simulation results followed by discussion and conclusion in sections "Discussion" and "Conclusion," respectively.

Methods

Needle–tissue system

A conventional configuration of a needle insertion procedure into the soft tissue is depicted in Figure 1. The goal of the insertion is to steer and control the needle to reach a target located deep inside the prostate. As evident in the ultrasonic images, the prostate is anchored around the pubic bone that causes the rotation of prostate tissue upon needle insertion.[31] If a prismatic movement of a nonflexible needle is considered, the dynamics equation of the system in the insertion frame ($Y_{ins} - X_{ins}$) can be written as follows

$$M\ddot{x} + sign(\dot{x}) \int_L \vec{v}^T . f(x, \dot{x}) dx = u(t) \quad (1)$$

where x is the needle tip position in the insertion frame ($Y_{ins} - X_{ins}$), M_n is the needle mass, $f(x, \dot{x})$ is the force per length applied by the tissue to the needle at dx (Figure 1(a)) as a function of the needle position (x)

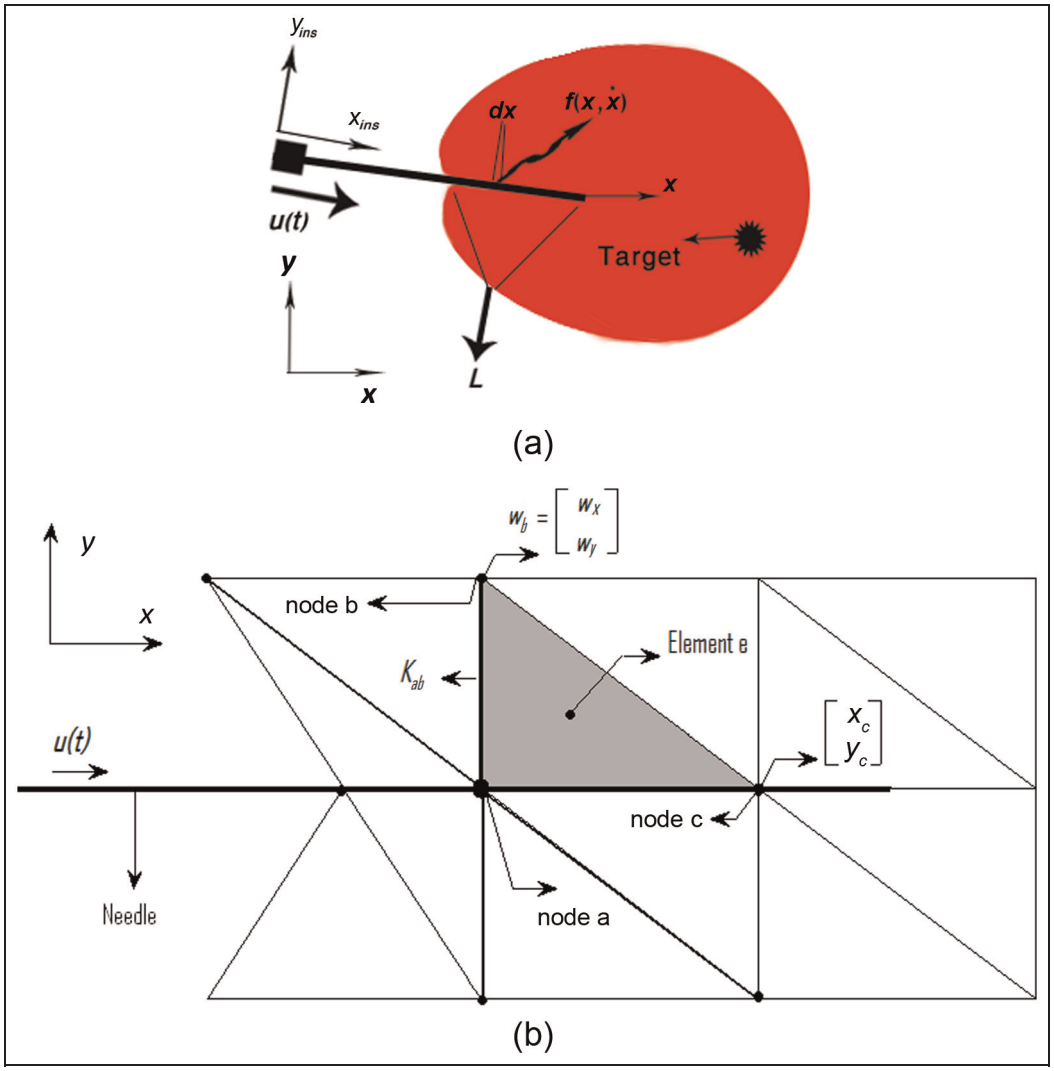

Figure 1. (a) A conventional needle insertion configuration and (b) FEM-based realization of equation (3). The force applied to the needle at node *a* can be calculated knowing the displacement vector of the adjacent node (w_b) and the local stiffness matrix defined between nodes *a* and *b* (K_{ab}). The coordinates of the nodes are $[X_aY_a]^T$ for node *a*, $[X_bY_b]^T$ for node *b*, and $[X_cY_c]^T$ for node *c*, and the displacement vectors of the nodes are w_a for node *a*, w_b for node *b*, and w_c for node *c*.

and velocity ($\dot{x}$)[18] while the *sign* function preserves the alignment of the needle direction and the force applied to it. Furthermore, $\vec{v}$ is the unit vector along the direction of the insertion projecting the force along the needle shaft and $u(t)$ is the force applied to the base of the needle in order to insert the needle into the tissue, namely, the "control law."

Model-based force estimation for the needle insertion

To measure applied force to the needle by the tissue, one may employ a force sensor at the base of the needle. However, such approach may prove to be cumbersome due to the calibration difficulties and presence of noise. Besides, the distribution of the force along the needle shaft can at best be indirectly measured by such force sensor utilization. Other indirect methods such as force observer are proposed to estimate the force applied to the needle by measuring the velocity and position of the needle.[32]

The significance of the estimation of the force distribution along the needle shaft is demonstrated when the flexible and bevel-tip needles are used, and the needle path inside the tissue is no longer a straight path but a curved path. Subsequently, the curvature of the needle path inside the tissue can be approximated more effectively using the estimated lateral forces, and the algorithms using the needle curvature for steering[33] will benefit by this approach.

A model-based method is used in this study for the estimation of the applied force to the needle. This is due to the fact that tissue deformation and applied external force to the tissue are related as governed by the tissue model. Thereby, tissue deformation may be utilized to estimate the applied external force and vice versa. The advantage of this method is that in addition to the estimation of the distribution of the forces along the needle

shaft, this model-based force measuring method can be exploited in the adaptive controller.

As a discrete model of the tissue is used in the context of FEM, the integral over the needle length can be substituted with the summation of the forces applied to the needle by the nodes of the soft tissue mesh

$$M\ddot{x} + sign(\dot{x}) \sum_{a=1}^{n(x)} \vec{v}^T . \overrightarrow{f_a} = u(t) \tag{2}$$

where $\overrightarrow{f_a}$ is the force applied by the ath node of the soft tissue mesh that is in contact with the needle, $n(x)$ is the number of tissue nodes in contact with the needle and obviously is a function of the x (i.e. the number of contact nodes increases as needle is inserted deeper into the tissue). In the case of the 2D and linear FEM for the tissue, the force applied to each contact node (f_a) is the sum of the scalar product of the local stiffness matrix and the displacement vector of the node adjacent to the contact node[34] (including contact node itself)

$$\overrightarrow{f_a} = \sum\nolimits_{b=1}^{m(a)} K_{ab}(\Theta).w_b; \quad w_b = \begin{bmatrix} w_{x_b} \\ w_{y_b} \end{bmatrix} \tag{3}$$

where $K_{ab}(\Theta)$ is the local stiffness matrix defined between node a (in contact with the needle) and node b (connected to node a in the tissue mesh that includes a itself) and is a function of the unknown parameters (Θ), $m(a)$ is the number of the nodes connected to the node a, w_b is the displacement vector of the adjacent node that consists of w_{x_b} and w_{y_b}, which are the displacement of the node b in x-direction and y-direction, respectively. Figure 1(b) depicts the FEM realization of the needle–tissue interaction forces.

The local stiffness matrix can be written as[34]

$$\begin{aligned} &K_{ab}(\Theta) = \frac{t}{4\Delta} \times B^T(a) \times D \times B(b); \\ &B(a) = \begin{bmatrix} \alpha_a & 0 & \beta_a \\ 0 & \beta_a & \alpha_a \end{bmatrix}; \quad D = \begin{bmatrix} \lambda + 2\mu & \lambda & 0 \\ \lambda & \lambda + 2\mu & 0 \\ 0 & 0 & \mu \end{bmatrix} \\ &\alpha_a = Y_b - Y_c \quad \alpha_b = Y_c - Y_a \\ &\beta_a = X_b - X_c \quad \beta_b = X_c - X_a \\ &\lambda = \frac{E\upsilon}{(1-\upsilon^2)} \quad \mu = \frac{E(1-\upsilon)}{2(1-\upsilon^2)} \end{aligned} \tag{4}$$

where t is the thickness of the tissue; Δ is the area of each triangular element of the tissue mesh; E is Young's modulus; υ is Poisson's ratio; λ and μ are the Lamé parameters; α_a, α_b, β_a, and β_b are the functions of the position of the element's nodes of which node a is a part (e.g. referring to Figure 1, node a is a part of the mesh element e). Here X_a, X_b, and X_c are the x coordinates and Y_a, Y_b, and Y_c are the y coordinates of element e in the world frame of $X - Y$ for nodes a, b, and c, respectively.

The needle dynamics can now be written as

$$M\ddot{x} + sign(\dot{x}) \sum_{a=1}^{n(x)} \sum_{b=1}^{m(a)} \vec{v}^T . K_{ab}(\Theta) \times w_b = u(t) \tag{5}$$

To derive the desired control rule, the external force term is parameterized with respect to the unknown parameters (Θ).

If Θ denotes the unknown tissue parameters of $\begin{bmatrix} \lambda \\ \mu \end{bmatrix}$, by using the equation (4) the double summation in equation (5) can be parameterized with respect to Θ as

$$\begin{aligned} &sign(\dot{x}) \sum_{a=1}^{n(x)} \sum_{b=1}^{m(a)} \vec{v}^T . K_{ab}(\Theta) \times w_b = sign(\dot{x}) \\ &\sum_{a=1}^{n(x)} \sum_{b=1}^{m(a)} \vec{v}^T . y_{ab}(w_b)\Theta = \vec{v}^T . \varphi(x, \dot{x}, w)\Theta \\ &y_{ab}(w_b) = \\ &\begin{bmatrix} w_{y_b}\beta_b\alpha_a + w_{x_b}\alpha_a\alpha_b & w_{y_b}\beta_a\alpha_b + 2w_{x_b}\alpha_a\alpha_b + w_{x_b}\beta_a\beta_b \\ w_{x_b}\beta_a\alpha_b + w_{y_b}\beta_a\beta_b & w_{x_b}\beta_b\alpha_a + 2w_{y_b}\beta_a\beta_b + w_{y_b}\alpha_a\alpha_b \end{bmatrix} \\ &\varphi(x, \dot{x}, w) = sign(\dot{x}) \sum_{a=1}^{n(x)} \sum_{b=1}^{m(a)} y_{ab}(w_b) \end{aligned} \tag{6}$$

where $y_{ab}(w_b)$ is a function of the tissue deformation and the position of the mesh nodes.

Finally by denoting $\varphi(x, \dot{x}, w)\Theta$ along the $\vec{v}$ (insertion direction) or $\varphi_v(x, \dot{x}, w)\Theta$

$$M\ddot{x} + \varphi_v(x, \dot{x}, w)\Theta = u(t) \tag{7}$$

Sliding mode control

To design the control law, equation (7) is converted to the state-space representation ($x_1 = x$, $x_2 = \dot{x}$)

$$\begin{aligned} \dot{\chi} &= \begin{bmatrix} \dot{x}_1 \\ \dot{x}_2 \end{bmatrix} = f(\chi, t) + Bu(t) \\ &= \begin{bmatrix} x_2 \\ -\dfrac{\varphi_v(x_1, x_2, w)\Theta}{M} \end{bmatrix} + \begin{bmatrix} 0 \\ \dfrac{1}{M} \end{bmatrix} u(t) \end{aligned} \tag{8}$$

Following the standard design procedure of the sliding mode control (SMC) to derive the control law,[35] a switching manifold is selected as

$$s = x_2 + (x_1 - x_d) = \dot{x} + (x - x_d) \tag{9}$$

where x_d is the target location in the insertion frame. Furthermore, due to the tissue deformation and the target movement, x_d is not constant.

Next, the "equivalent control signal" u_{eq} introduced satisfies the system dynamics of $\dot{s} = 0$

$$u_{eq} = -\left(\frac{\partial s}{\partial \chi} B\right)^{-1} \left(\frac{\partial s}{\partial \chi} f(\chi, t)\right) \tag{10}$$

which according to the formulation of the needle dynamics can be derived as

$$u_{eq} = -Mx_2 + \varphi_v(x_1, x_2, w)\Theta = -M\dot{x} + \varphi_v(x, \dot{x}, w)\Theta \quad (11)$$

Inverse dynamics controller

If the soft tissue parameters are available, the inverse dynamics can be used to control the needle in the soft tissue. It is conventional to add an error-dependent term to the equivalent control signal (u_{eq}), which was designed by sliding mode approach in the previous section, and the control law proceeds as follows

$$u = u_{eq} - Ks = -M\dot{x} + \varphi_v(x, \dot{x}, w)\Theta - Ks \quad (12)$$

where $K > 0$ is a gain of the error term. By substituting u in equation (7), the closed-loop equation becomes

$$M\ddot{x} + \varphi_v(x, \dot{x}, w)\Theta = -M\dot{x} + \varphi_v(x, \dot{x}, w)\Theta - Ks \quad (13)$$

Since

$$\dot{s} = \ddot{x} + \dot{x} - \dot{x}_d \quad (14)$$

The closed-loop equation simplifies to

$$M\dot{s} + Ks = 0 \quad (15)$$

It is shown that the nonlinear term of the dynamics equation is omitted through the usage of the inverse dynamics approach, so it is easy to show that the system is closed-loop stable. Hence, by choosing the classic Lyapunov function and derivation of this function along the closed-loop system trajectories, it can be written as

$$V = \frac{1}{2}Ms^2 \Rightarrow \dot{V} = M\dot{s}s = -Ks^2 \leqslant 0 \quad (16)$$

It can be deduced that the closed-loop system is globally stable, and the proof of asymptotical stability is achieved using Barbălat Lemma.[36] Note that when the nominal parameters of the soft tissue are unknown, the control law would be the same as equation (12) except that the Θ (nominal tissue parameters) will be replaced by $\hat{\Theta}$ (estimation of the tissue parameters).

Adaptive control

Another approach to tackle the uncertainty due to the unknown parameters is to use adaptive controller. In this approach, the employed control law is similar to the inverse dynamics approach with the estimation of the unknown parameters ($\hat{\Theta}$). The stability of the closed-loop system is achieved through updating unknown parameters.

By choosing the control law as

$$u = -M\dot{x} + \varphi_v(x, \dot{x}, w)\hat{\Theta} - Ks \quad (17)$$

the closed-loop system becomes

$$M\dot{s} + Ks = \varphi_v(x, \dot{x}, w)\hat{\Theta} \quad (\tilde{\Theta} = \hat{\Theta} - \Theta) \quad (18)$$

To obtain the update law for the parameters, the function V is chosen as follows

$$V = \frac{1}{2}Ms^2 + \frac{1}{2}\tilde{\Theta}^T\Lambda\tilde{\Theta} \Rightarrow \dot{V} = M\dot{s}s + \dot{\tilde{\Theta}}^T\Lambda\tilde{\Theta} = -Ks^2 + s\varphi_v(x, \dot{x}, w)\tilde{\Theta} + \dot{\tilde{\Theta}}^T\Lambda\tilde{\Theta} \quad (19)$$

where Λ is the gain for updating the unknown parameters.

Initially, the expression $s\varphi_v(x, \dot{x}, w)\tilde{\Theta} + \dot{\tilde{\Theta}}^T\Lambda\tilde{\Theta}$ is set to zero to obtain the law for updating the unknown parameter. In addition, it is assumed that the nominal parameters (Θ) are constant, or

$$\left(s\varphi_v(x, \dot{x}, w) + \dot{\tilde{\Theta}}^T\Lambda\right)\tilde{\Theta} = 0 \overset{\text{if } \Theta \text{ is constant}}{\Rightarrow} \dot{\tilde{\Theta}} = \dot{\hat{\Theta}} = -\Lambda^{-T}s\varphi_v(x, \dot{x}, w) \quad (20)$$

The update law in the discrete time can be written as

$$\hat{\Theta}(t+1) = \hat{\Theta}(t) - t_s \times \Lambda^{-T}s\varphi_v(x, \dot{x}, w) \quad (21)$$

where t_s is the sampling time of the simulation run.

By omitting the second and third terms of $\dot{V}$ in equation (17), it can be written as

$$\dot{V} = -Ks^2 \leqslant 0 \quad (22)$$

Proof on the stability of the above system is given by the Barbălat Lemma.[36]

Results

Two different needle control approaches are performed in simulation to investigate the feasibility of the proposed methods. Initially, inverse dynamics with parameter uncertainty is utilized to represent the system performance under inaccurate tissue mechanical parameter estimation. Next, adaptive controller is implemented to study the performance of the system with a further consideration of tissue parameters' estimation. The needle–tissue model used in the simulations[29] employs the 2D and linear FEM as the model for tissue and the stick–slip as the needle–tissue contact model.[17] According to Ophir et al.,[30] in all simulations, the nominal tissue parameters (mean values) for Young's modulus are assumed to be 100 kPa and Poisson's ratio is assumed to be 0.490. To simulate the cases with uncertainty in tissue parameter, Young's modulus was swept between 80 and 120 kPa with the step size of 10 kPa. For Poisson's ratio, the selected values were 0.480, 0.490, 0.495, and 0.499.[30]

In order to compare the performance of the system in different conditions (regarding parameter uncertainty and controller gain), two performance indices are introduced. The error along the y-axis is utilized as a measure for comparison of the system behavior in different

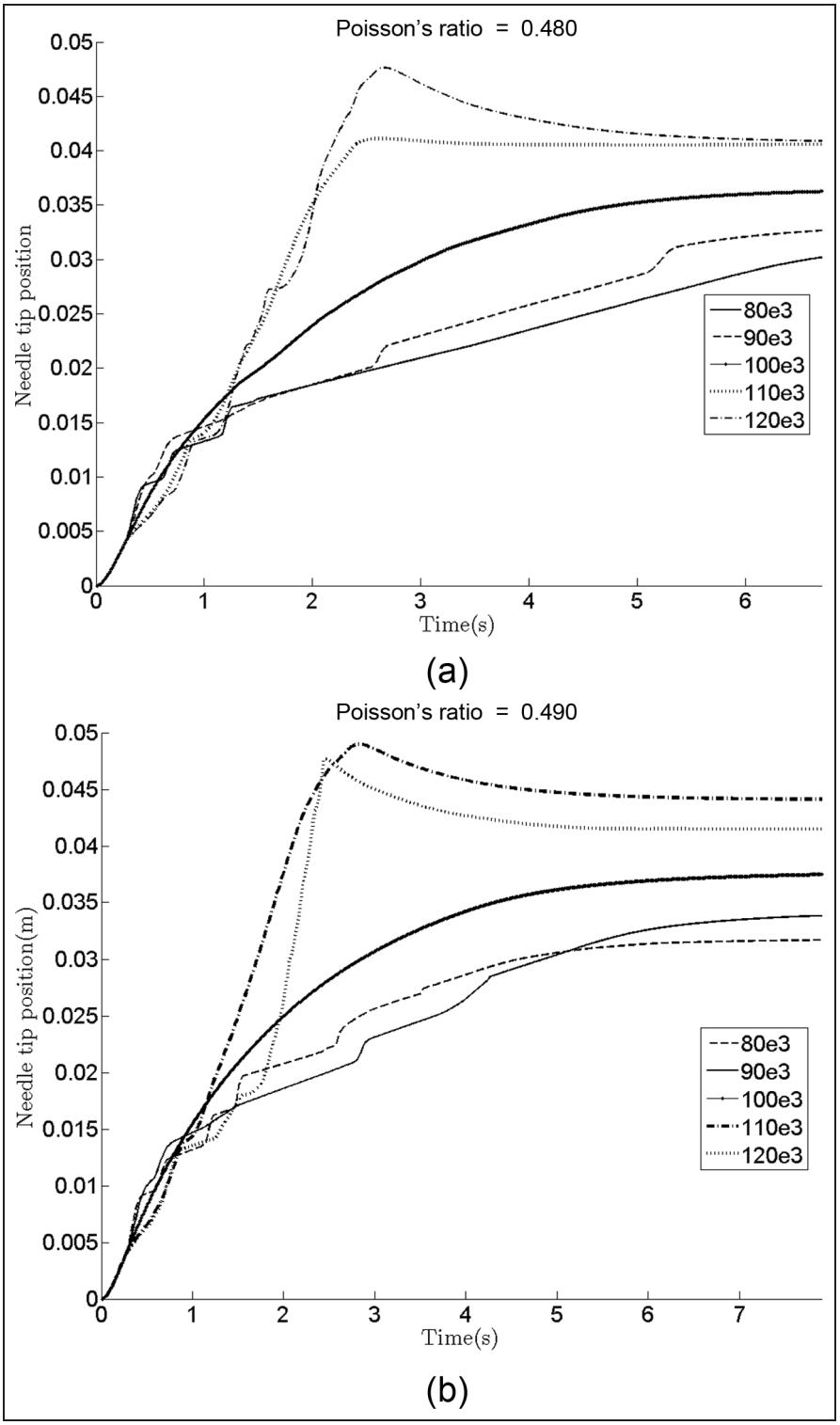

Figure 2. Needle tip position (*X*-direction) using inverse dynamics with controller gain (*K*) of 1 for different Young's moduli and Poisson's ratios of (a) 0.480 and (b) 0.490

conditions. The other index is based on the jerk of the movement, which is the second derivative of the needle velocity depicting the smoothness of the velocity.

In the following simulations, the location of the target is assumed to be $[2.5\ 2.5]^{T}$ cm deep inside the tissue, in the world frame of *X*–*Y* of Figure 1(b).

Inverse dynamics with parameter uncertainty

Here, uncertainty in tissue mechanical properties, namely, Young's modulus and Poisson's ratio, is evaluated simultaneously and controller gain (*K*) is set to 1. Figure 2 shows the needle tip position for uncertainty in the parameters alongside with the case of no

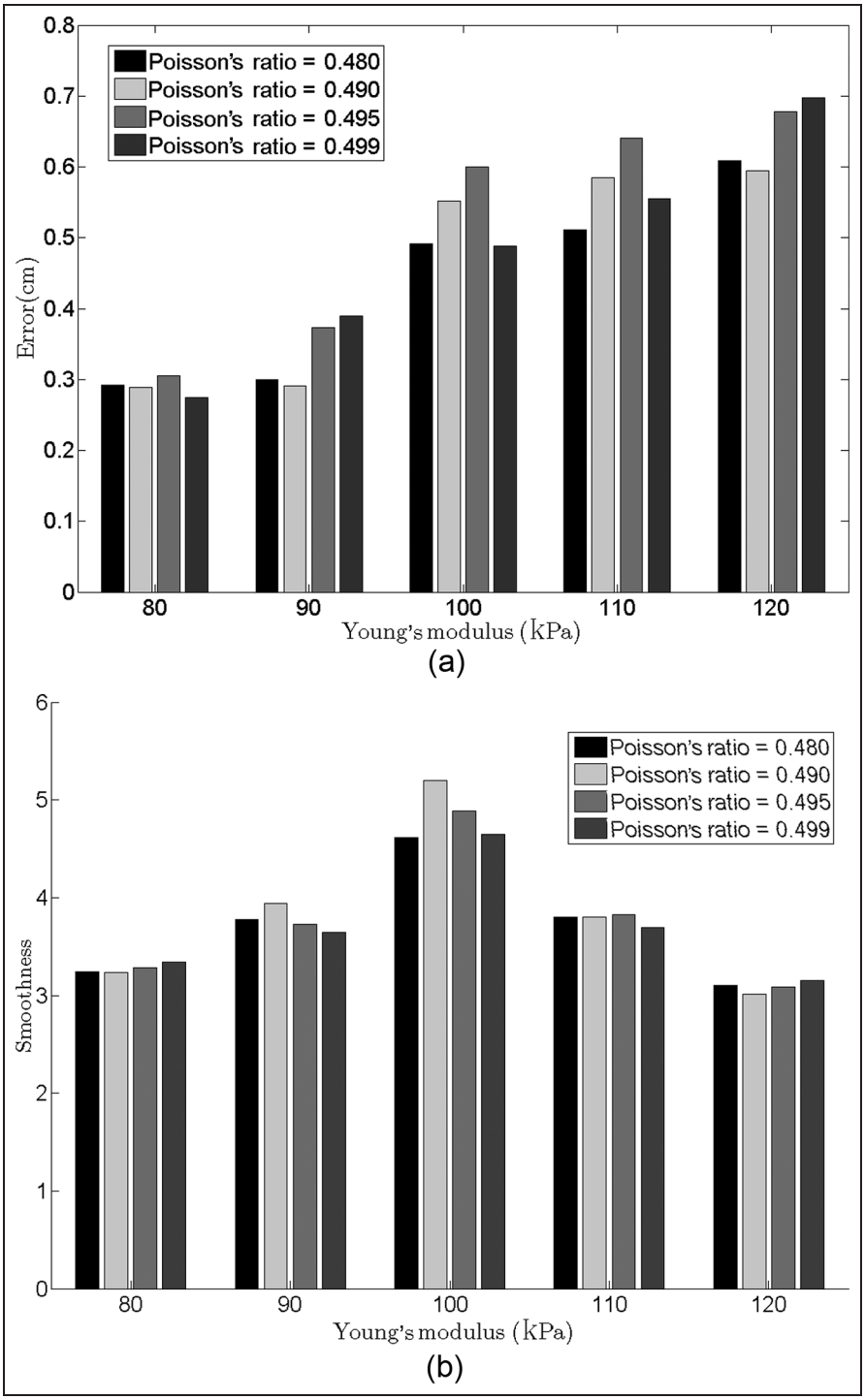

Figure 3. Performance indices of (a) position error (*y*-direction) and (b) smoothness using inverse dynamics for different Poisson's ratios and Young's moduli.

parameter uncertainty, which is depicted in the bold curve of Figure 2(b). It is shown that the inaccurate estimation of the parameters can noticeably degrade the system behavior with a slower response or an overshoot in the response. In addition, Figure 3 shows the performance indices in the presence of uncertainty in both parameters. The divergence from the nominal parameters leads to considerable changes in velocity's smoothness. The larger Young's modulus causes larger *y*-direction position errors while the effect of Poisson's ratio is comparatively minimal.

Effect of the controller gain

The effect of the controller gain (K) on the performance of the system, using inverse dynamics control with parameter uncertainty, is also investigated. Through extensive simulation runs, three gains were selected, namely, 1, 5, and 10.

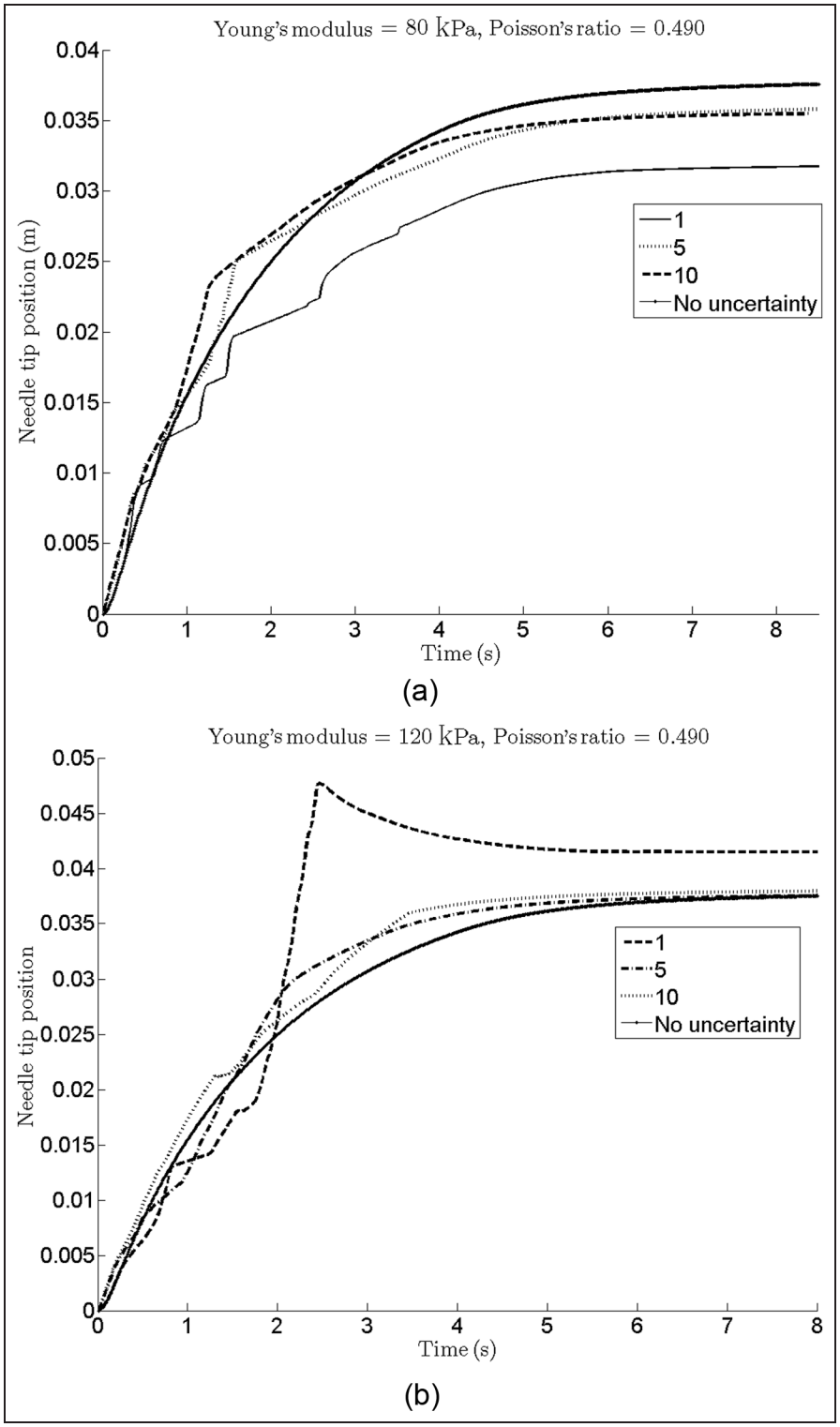

Figure 4. Needle tip position (*X*-direction) obtained by inverse dynamics with different gains and (a) Young's modulus = 80 kPa and Poisson's ratio = 0.490 and (b) Young's modulus = 120 kPa and Poisson's ratio = 0.490. The case with no parameter uncertainty with $K = 1$ is also shown by the bold line as baseline.

Figure 4 shows the needle tip position obtained for inverse dynamics method with different values of Young's modulus and Poisson's ratio of 0.490. Moreover, the result with $K = 1$ and no parameter uncertainty is also shown for comparative purposes.

As depicted in Figure 4, increasing the gain causes a considerable improvement in the system performance, that is, the latency of the response is lessened in the case of underestimation of Young's modulus (Figure 4(a)) and the overshoot is vanished in the case of overestimation of Young's modulus (Figure 4(b)).

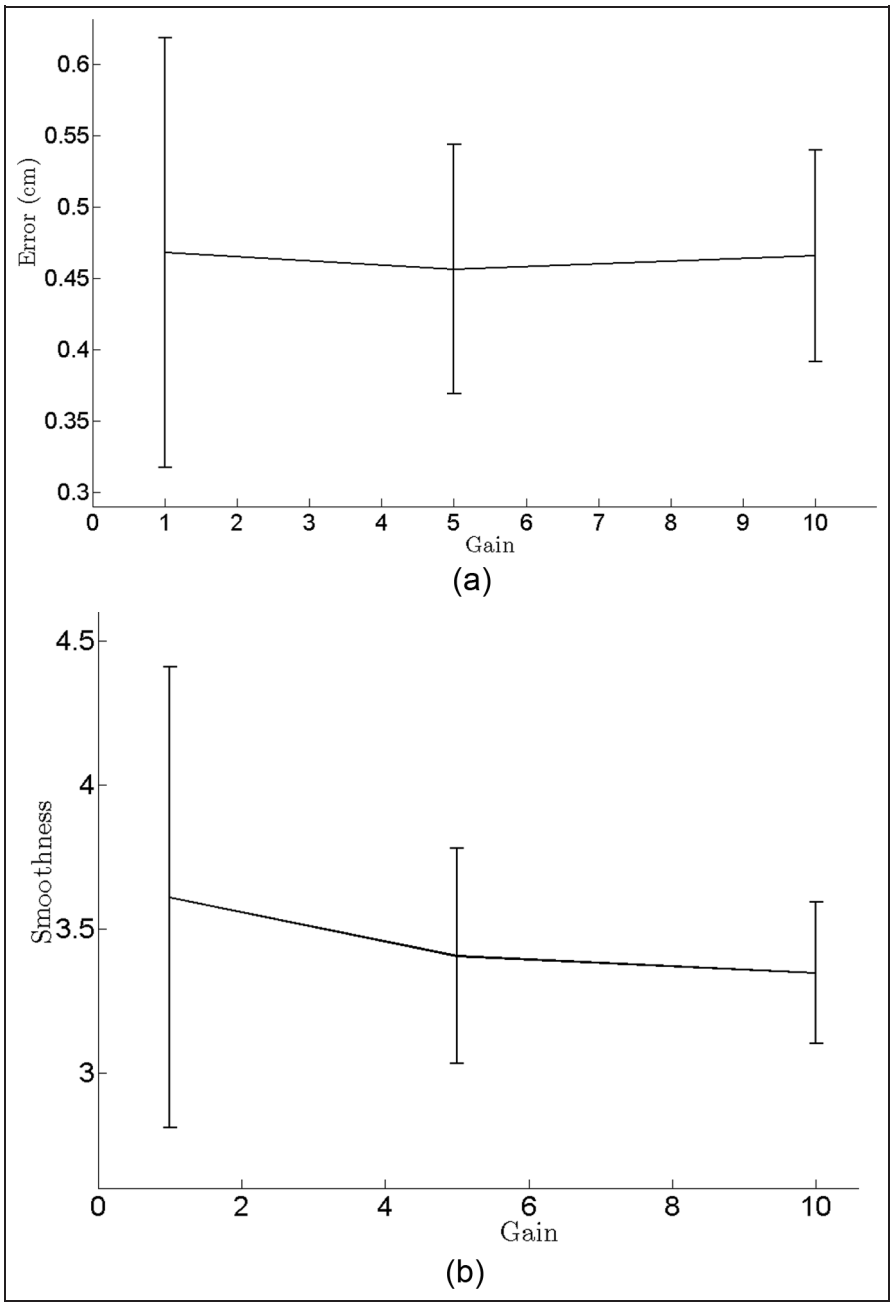

Figure 5. Performance indices of (a) position error (*y*-direction) and (b) smoothness for different gains using the inverse dynamics for Young's modulus and Poisson's ratio combinations of figure 3.

Figure 5 shows the performance indices for different gains and different amounts of uncertainty in tissue parameters. It can be deduced from Figure 5 that increasing the gain reduces the variance and upper bound of the smoothness of the needle velocity and the error.

Adaptive controller

As depicted in the previous section, the inaccurate estimation of the tissue parameters degraded the system performance dramatically. As a solution, adaptive controller was proposed and simulated accordingly.

The effects of parameter uncertainty on the performance were investigated using a similar approach noted for the inverse dynamics method. Furthermore, the effect of the gain for updating the unknown parameters was investigated. To do so, the value of this parameter is swept from 1 to 10^{10} with step of 10. It was observed that the performance of the system does not change for values smaller than 10^8, so the results for the gain for updating the unknown parameters of 10^8, 10^9, and 10^{10} along with inverse dynamics, carrying the gain of zero, are shown.

Figure 6 shows the needle tip position with different tissue parameters. As it can be shown that the adaptive controller response is faster than the inverse dynamics in the case of underestimation of Young's modulus (Figure 6(a)) and the overshoot is decreased in the case of

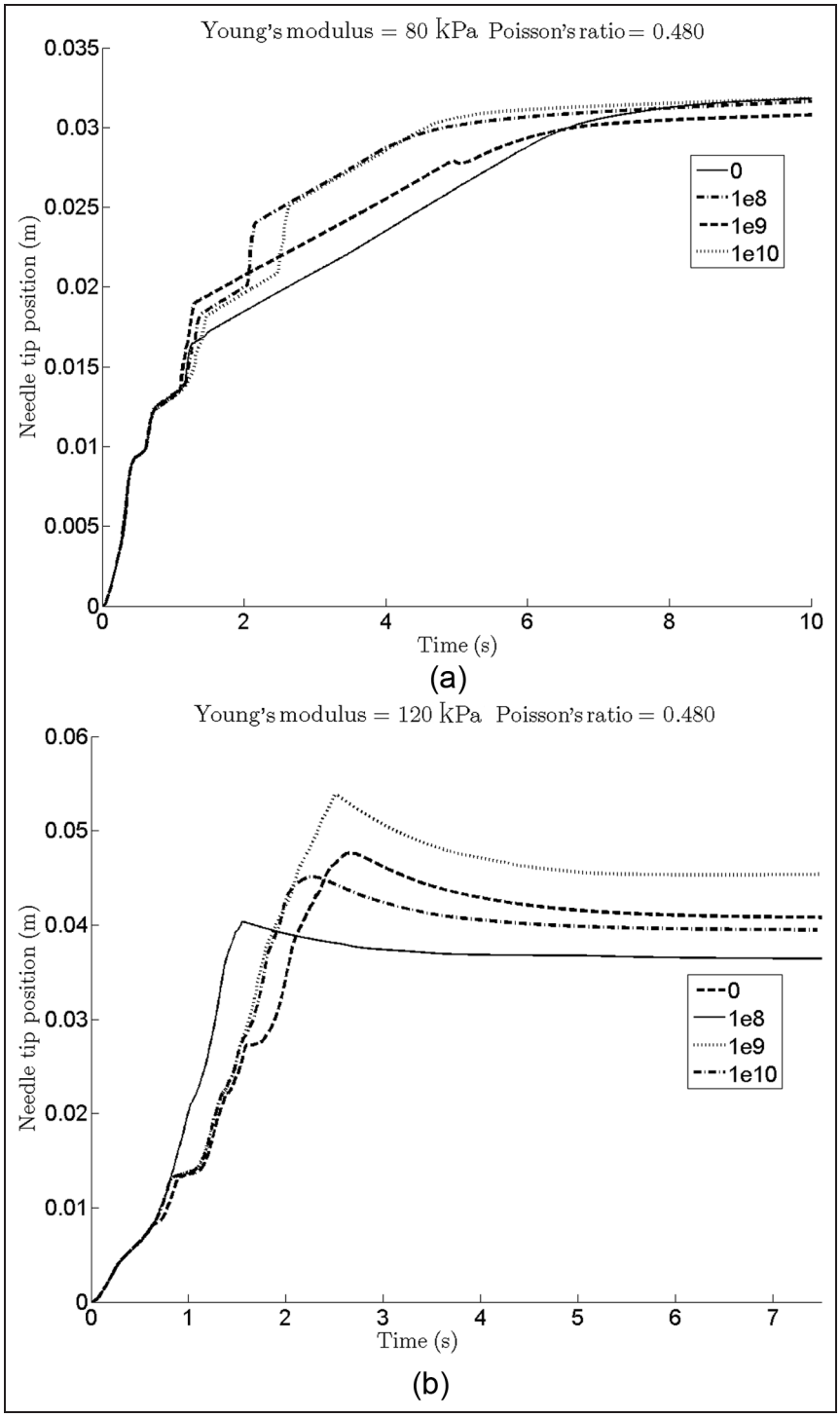

Figure 6. Needle tip position (*X*-direction) using adaptive controller with controller gain (K = 1) and different gains for updating the unknown parameters for (a) Young's modulus = 80 kPa and Poisson's ratio = 0.480 and (b) Young's modulus = 120 kPa and Poisson's ratio = 0.480.

overestimating Young's modulus (Figure 6(b)) if the gain for updating the unknown parameters is chosen correctly.

The role of the controller gain (K) for the adaptive controller is also investigated here for three different gains of 1, 5, and 10. Figure 7 shows the performance indices for different gains and pairs of elastic moduli. Here, the results depict similar trend as the inverse dynamics case, that is, increasing the gain decreases the variance and upper bound of the smoothness of the needle velocity and the y-direction position error.

Discussion

The proposed needle–tissue system was simulated by using the proposed simulation algorithm and the discussed controllers. The simulations endorsed the

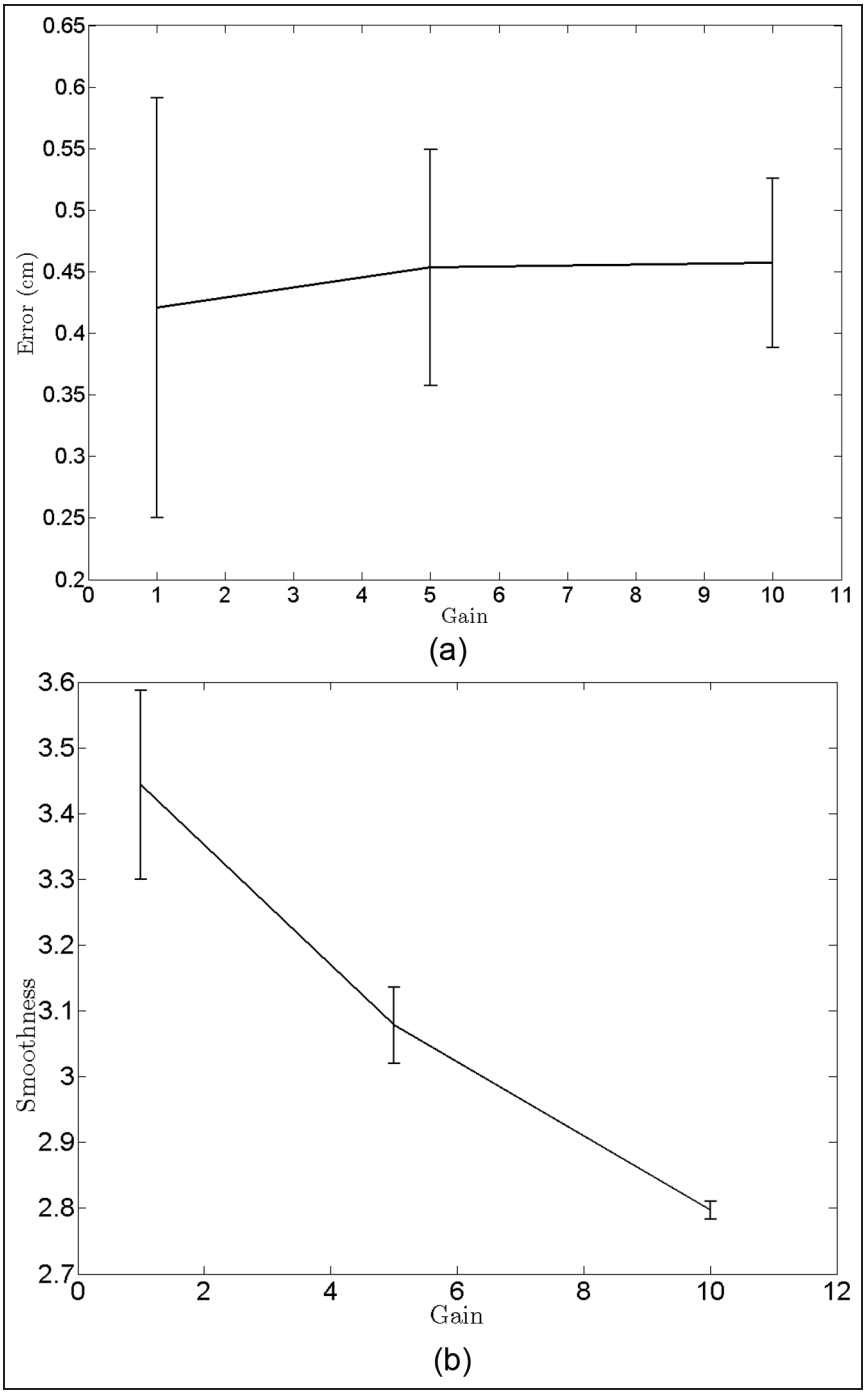

Figure 7. The performance indices of (a) position error (*y*-direction) and (b) smoothness for different gains using adaptive controller for Young's moduli and Poisson's ratios of figure 3 and gain for updating the unknown parameters of 10^{10}.

stability analysis discussed in the previous sections and the reaching error along the insertion direction always tends to zero.

To consider the effect of inaccurate estimation of the tissue parameters in needle control, the inverse dynamics method with uncertainty in the tissue parameters was also investigated. For the uncertainty in Young's modulus, two types of degraded system responses were observed: the delayed and slow response due to the underestimation of Young's modulus and overshoot due to the overestimation of Young's modulus. This can be explained by taking into account that the control signal as proposed in equation (12) was the external driving force applied to the needle to insert it into the tissue. When the controller underestimated Young's modulus, the generated control signal was smaller as if it was being generated for a softer tissue, thereby resulting in a slower response. In contrary, when the controller overestimated Young's modulus, the generated control signal was larger because it was

being generated for a stiffer tissue and thereby more force was needed to drive into the tissue, and the result was overshooting the target. It was further shown that deviation from the nominal tissue Young's modulus causes less smoothness in the needle velocity, and increase in Young's modulus causes more target-reaching errors. The larger Young's modulus causes a larger control signal, which consequently increases the tissue deformation and rotation and leads to larger error in the y-direction.

The inaccurate estimation of Poisson's ratio introduced slight changes in the system behavior with a minor change in smoothness of the needle velocity and the error. The effect of the controller gain (K) on the system response was also investigated in the case of inverse dynamics with uncertainty. It was shown that increasing the gain of the controller improved the needle tip position's profile by suppressing the overshoot in the case of Young's modulus overestimation and improved the latency in the case of Young's modulus underestimation. It was also observed that increasing the controller gain decreased the smoothness of the velocity and the variance and the upper bound of the reaching error. The improvement in the response can be explained by separating the terms in the control signal in equation (12), into two categories, namely, dynamics-based term of $\varphi_v(x, \dot{x}, w)\hat{\Theta}$ and kinematics-based terms.

Increasing K accentuates the effect of the kinematics-based terms and reduces the effect of the dynamics-based term that contains the parameter mismatch. The adaptive controller was proposed in section "Methods." The simulations were done in two categories, namely, the role of the controller gain (K) and the role of the gain for updating the unknown parameters (Λ). To compare the performance of the adaptive controller with the inverse dynamics methods, the adaptive control with different gains for updating the unknown parameters were simulated and compared to the results of the inverse dynamics method. It was observed that the performance of the adaptive controller was better than that of the inverse dynamics if the gain for updating the unknown parameters would be chosen correctly, that is, the latency for underestimation of Young's modulus and the overshoot for overestimation were compensated. On the other hand, the performance indices for the adaptive controller were close to those of the inverse dynamics but slightly better for the adaptive controller with the appropriate gains for updating the unknown parameters. The role of the controller gain (K) was also investigated, and the results had the same characteristics as the inverse dynamics results.

The proposed scheme can be extended to 2D; however, for 3D extension, the finite element modeling of the behavior of the soft tissue should also be simulated in 3D. There are two possible approaches for the expansion of the current model to 2D, namely, assumptions of a rigid needle and a flexible needle. In the following, we will briefly explain this aspect of the problem in detail.

1. *Assumption of a rigid needle*: There are three issues that should be approached regarding 2D dynamics model and control of the needle.

a. *Derivation of the force applied by the tissue to the needle*: Based on equation (5), the force applied by the tissue to the needle, namely, the term with double summation, is actually calculated in 2D; however, the unique vector $\vec{v}$ projects this 2D force in the direction of insertion. Simply omitting $\vec{v}$ yields the force applied to the needle in the nodes that are in contact with the tissue in 2D.

b. *Needle dynamics*: Assuming a rigid needle, its dynamical model can be derived by considering the needle as a prismatic joint modeling the insertion along the x-axis, currently considered in this study, and a rotational joint as the second degree of freedom along the axis perpendicular to the insertion plane, to compensate the off-path errors. The force applied by the tissue can be incorporated in this dynamics equation to model the behavior of the needle.

c. *Control*: The control signal now has two components, the x-direction force of the needle that penetrates the tissue and the torque applied to the needle's base to compensate the off-path errors. Once the dynamics of the needle is derived, the control approach can be designed following the same procedure proposed in this article.

While this formulation seems feasible, the assumption of needle rigidity is not appropriate since the lateral force exerted to the base of the needle in the y-direction causes needle deflection. This deflection voids the accuracy of the dynamics modeling. However, the assumption of the rigid needle can still be valid if the needle is undergoing only the insertion forces in the x-direction.[27]

2. *Assumption of a flexible needle*: According to the previous discussion, it seems that for 2D needle manipulation, a flexible model for the needle dynamics is crucial. However, this assumption dramatically changes the current framework proposed in this study since the dynamics of a flexible needle is fundamentally different compared to a rigid one.

Conclusion

This study considered a novel approach toward evaluation of controller design in driving a needle into prostate tissue. The proposed scheme introduced and simulated a model-based dynamics equation of the needle–tissue system. Inverse dynamics and adaptive controllers were investigated and further compared in order to address the role of tissue parameter estimation in needle insertion problem and to highlight the role of different controller gains. It was shown that parametric mismatch due to the uncertainty in the soft tissue's parameter can have drastic effects in the system behavior. It was further demonstrated that the velocity

smoothness and x-direction and y-direction position errors for the adaptive controller were close to that of the inverse dynamics but slightly better for the former with adaptive fine-tuning of the gain for updating the unknown parameters.

We hope that the current and similar studies would eventually lead to semiautomatic procedures, similar to other well-practiced ones, where under physician supervision, a much better manipulation would result. This study can be regarded as a first step in such procedures.

Funding

This research received no specific grant from any funding agency in the public, commercial, or not-for-profit sectors.

Conflict of interest

The authors declare that they have no conflicts of interest.

References

1. Wei Z, Wan G, Gardi L, et al. A Fenster, robot-assisted 3D-TRUS guided prostate brachytherapy: system integration and validation. *Med Phys* 2004; 31: 539–548.
2. Danese D, Sciacchitano S, Farsetti A, et al. Diagnostic accuracy of conventional versus sonography-guided fine-needle aspiration biopsy of thyroid nodules. *Thyroid* 1998; 8: 15–21.
3. Rizun PR, McBeth PB, Louw DF, et al. Robot-assisted neurosurgery. *Semin Laporasc Surg* 2004; 11: 99–106.
4. Abolhassani N, Patel R and Moallem M. Needle insertion into soft tissue: a survey. *Med Eng Phys* 2007; 29: 413–431.
5. Alterovitz R, Goldberg K, Pouliot J, et al. Sensorless planning for medical needle insertion procedures. *Intelligent Robots and Systems, (IROS 2003). Proceedings. IEEE/RSJ International Conference*, Las Vegas, NV, 2003, vol. 3, pp. 3337–3343.
6. DiMaio SP and Salcudean SE. Needle insertion modeling and simulation. *IEEE T Robot Autom* 2003; 19: 864–875.
7. Alterovitz R, Pouliot J, Taschereau R, Hsu IJ, Goldberg K. Simulating needle insertion and radioactive seed implantation for prostate brachytherapy. *Studies in health technology and informatics*, 2003, pp. 19–25.
8. Goksel O, Salcudean SE and DiMaio SP. 3D simulation of needle-tissue interaction with application to prostate brachytherapy. *Comput Aided Surg* 2006; 11: 279–288.
9. Goksel O, Salcudean SE, DiMaio SP, et al. 3D needle-tissue interaction simulation for prostate brachytherapy. Medical Image Computing and Computer-Assisted Intervention (MICCAI), Palm Springs, USA, 2005, pp. 827–834.
10. Dehghan E and Salcudean SE. Needle insertion point and orientation optimization in non-linear tissue with application to brachytherapy. *Robotics and Automation, IEEE International Conference*, Roma, Italy, April 2007, pp. 2267–2272.
11. Maurin B, Barbe L, Bayle B, et al. In Vivo Study of Forces During Needle Insertions. *Proceedings of the Medical Robotics, Navigation and Visualisation Scientific Workshop* 2004, Remagen, Germany, March 2004, pp. 415–422.
12. Simone C and Okamura AM. Modeling of needle insertion forces for robot-assisted percutaneous therapy. *Robotics and Automation, Proceedings. ICRA '02. IEEE International Conference*, Washington, DC, 2002, pp. 2085–2091.
13. Simone C. *Modelling of needle insertion forces for percutaneous therapies*. Master's Thesis, Johns Hopkins University, Baltimore, MD, 2002.
14. Okamura AM. Force modeling for needle insertion into soft tissue. *IEEE Trans Biomed Eng* 2004; 51: 1707–1716.
15. Podder TK, Sherman J, Clark DP, et al. Evaluation of robotic needle insertion in conjunction with in vivo manual insertion in the operating room. *Robot and Human Interactive Communication, IEEE International Workshop*, Nashville, TN, 2005, pp. 66–72.
16. Karnopp D. Computer simulation of stick-slip friction in mechanical dynamic systems. *Trans ASME J Dyn Syst Meas Contr* 1985; 107: 100–103.
17. DiMaio SP and Salcudean SE. Interactive simulation of needle insertion models. *IEEE Trans Biomed Eng* 2005; 52: 1167–1179.
18. Crouch JR, Chad MS, Wainer J, Okamura AM. A velocity-dependent model for needle insertion in soft tissue. *Med Image Comput Comput Assist Interv (MICCAI)*, Palm Springs, CA, 2005, pp. 624–632
19. Dehghan E, Xu W, Zahiri-Azar R, et al. Modeling of needle-tissue interaction using ultrasound-based motion estimation. *Med Image Comput Comput Assist Interv (MICCAI)*, Brisbane, QLD, Australia, 2007, pp. 709–716.
20. DiMaio SP and Salcudean SE. Needle steering and motion planning in soft tissues. *IEEE T Bio-Med Eng* 2005; 52: 965–974.
21. Alterovitz R, Lim A, Goldberg K, et al. Steering flexible needles under Markov motion uncertainty. *Intelligent Robots and Systems, (IROS 2005). IEEE/RSJ International Conference*, Edmonton, AB, Canada, 2005, pp. 1570–1575.
22. Bertsekas DP. *Dynamic programming and optimal control*. 2nd ed. Athena Scientific, U.S.A., 2000.
23. Alterovitz R, Goldberg K and Okamura A. Planning for steerable bevel-tip needle insertion through 2D soft tissue with obstacles. *Robotics and Automation, ICRA IEEE International Conference*, Barcelona, Spain, 2005, pp. 1640–1645.
24. Webster RJ, Kim JS, Cowan NJ, et al. Nonholonomic modeling of needle steering. *Int J Robot Res* 2006; 25: 509–525.
25. Park W, Kim JS, Zhou Y, et al. Diffusion-based motion planning for a nonholonomic flexible needle model. *Robotics and Automation, ICRA IEEE International Conference on*, Barcelona, Spain, 2005, pp. 4600–4605.
26. Glozman D and Shoham M. Flexible needle steering and optimal trajectory planning for percutaneous therapies. *Proceedings of the international conference on Medical Image Computing and Computer-Assisted Intervention*. New York, NY, 2004, pp. 137–144.
27. Dehghan E and Salcudean SE. Needle insertion parameter optimization for brachytherapy. *IEEE T Robot* 2009; 25: 303–315.
28. Wood NA, Shahrour K, Ost MC, et al. Needle steering system using duty-cycled rotation for percutaneous kidney access. In: *International conference of the IEEE*

EMBS, Buenos Aires, Argentina, 31 August–4 September 2010.
29. Maghsoudi A and Jahed M. Multi-parameter sensitivity analysis for guided needle insertion through soft tissue. In: *Proceedings on IEEE EMBS Conference on Biomedical Engineering & Sciences (IECBES)*, Kuala Lumpur, Malaysia, 2010, pp. 97–100.
30. Ophir J, Alam SK, Garra B, et al. Elastography: ultrasonic estimation and imaging of the elastic properties of tissues. *Proc IMechE, Part H: J Engineering in Medicine* 1999; 213: 203–233.
31. Lagerburg V, Moerland MA, Van Vulpen M, et al. A new robotic needle insertion method to minimise attendant prostate motion. *Radiother Oncol* 2006; 80: 73–77.
32. Hacksel PJ and Salcudean SE. Estimation of environment forces and rigid-body velocities using observers. In: *Proceedings of the IEEE international conference on robotics and automation*, San Diego, CA, 1994, pp. 931–936.
33. Abolhassani N, Patel R and Ayazi F. Needle control along desired tracks in robotic prostate brachytherapy. *Systems, Man and Cybernetics, 2007. ISIC. IEEE International Conference on*, Montreal, Canada, 2007, pp. 3361–3366.
34. Zienkiewicz OC, Taylor RL and Zhu JZ. *The finite element method: its basis and fundamentals*. 6th ed. Elsevier Butterworth-Heinemann, United Kingdom, 2005.
35. Yu X and Kaynak O. Sliding-mode control with soft computing: a survey. *IEEE T Ind Electro* 2009; 56: 3275–3285.
36. Hassan KK. *Nonlinear systems*. 3rd ed. Prentice-Hall, U.S.A., 2002.